

1 **Supplementary Materials to “The Impact of Three-Dimensional Structure of Subduction Zone**  
2 **on Time-dependent Crustal Deformation Measured by HR-GNSS”**

3 Oluwaseun Idowu Fadugba<sup>1</sup>, Valerie J. Sahakian<sup>1</sup>, Diego Melgar<sup>1</sup>, Arthur Rodgers<sup>2</sup> and Roey  
4 Shimony<sup>1</sup>

5 (1) Department of Earth Sciences, University of Oregon, Eugene, OR

6 (2) Lawrence Livermore National Laboratory, Livermore, CA

7  
8 S1. GMSH fault geometry

9 We use GMSH, a 3-D finite element mesh generator (Geuzaine and Remacle, 2009) to  
10 generate a triangular mesh for the Kuril region of the Japan trench with the Slab2.0 datasets  
11 (Fig. S1). The mesh contains 4409 subfaults with depths ranging from 10 to 80 km. The area of  
12 each subfault varies from 0.67 to 167.3 km<sup>2</sup> but averages 57.4 km<sup>2</sup>. The smaller subfaults are to  
13 accommodate the curvature of the Japan trench. We output the mesh in two files needed by  
14 FakeQuakes (“Japan\_trench.fault” and “Japan\_trench.mshout”). The “Japan\_trench.fault” file  
15 contains important parameters such as the latitude, longitude, depth, strike, dip, length, width,  
16 and area of each subfault. The “Japan\_trench.mshout” file contains the coordinate of the  
17 centroid of each subfault including the coordinate of the nodes. The mesh files are available on  
18 Zenodo (<https://doi.org/10.5281/zenodo.7765170>).

19  
20 S2. Creating rfile

21 The unified 3D velocity model of Japan is a rfile (about 34 Gb size) spanning lateral  
22 extent of latitude from 30° to 47° North (~2040 km) and longitude from 129° to 147° East  
23 (~1440 km). The model maintains the 23 layers in the original 3D Japan Integrated Velocity  
24 Structure Model (Koketsu et al., 2008, 2009), each with constant P- and S-wave velocities ( $V_p$   
25 and  $V_s$ ), density ( $\rho$ ) and P- and S-wave quality factors ( $Q_p$  and  $Q_s$ ) (Table S3). The rfile has 5  
26 blocks with a constant horizontal spacing (hh) of 1 km, but the vertical grid spacing (hv)  
27 increases with depth. The rfile is available on Zenodo  
28 (<https://doi.org/10.5281/zenodo.7765170>).

29 The blocks information of the rfile are as follows:

- 30 1. Block 1: Topography/bathymetry ( $h_v = \text{no vertical spacing}$ ;  $h_h = 1 \text{ km}$ )
- 31 2. Block 2: -4 km to 30 km depth ( $h_v = 200 \text{ m}$ ;  $h_h = 1 \text{ km}$ ). The depth range of this block is
- 32 large enough to contain the highest point in topography and the lowest point in
- 33 bathymetry.
- 34 3. Block 3: 30 to 70 km ( $h_v = 300 \text{ m}$ ;  $h_h = 1 \text{ km}$ )
- 35 4. Block 4: 70 to 100 km ( $h_v = 400 \text{ m}$ ;  $h_h = 1 \text{ km}$ )
- 36 5. Block 5: 100 to 200 km ( $h_v = 500 \text{ m}$ ;  $h_h = 1 \text{ km}$ )

37

### 38 S3. Choosing the Grid spacing ( $h$ )

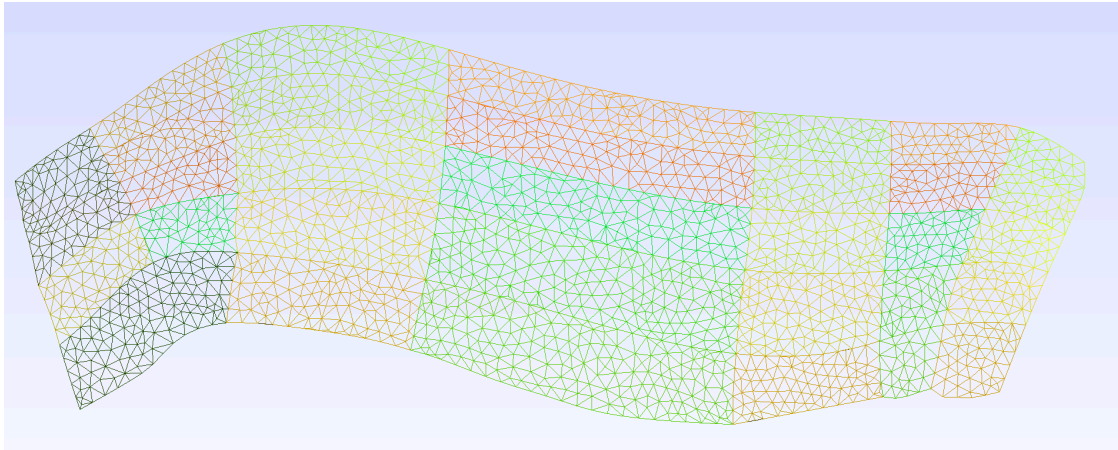
39 The choice of grid spacing is very important in SW4 as it determines the maximum  
40 frequency the model can resolve. It is related to the minimum shear wave velocity in the  
41 domain by  $h = \min V_s / (PPW \times f_{\max})$ ; where  $\min V_s$  is the minimum shear wave velocity, PPW is the  
42 Point Per Wavelength and  $f_{\max}$  is the maximum frequency in the simulation. According to SW4  
43 manual, the recommendation is that the PPW must be at least 8 for stable wave solutions. If we  
44 use a maximum frequency of 0.5 Hz while minimum  $V_s$  in the 3D velocity model is 350 m/s,  $h$  is  
45 87.5m. Based on the size of the domain geometry, this grid spacing will make the  
46 computational cost very expensive.

47 We increase the minimum shear wave velocity to 1200 m/s based on the average  $V_s$  in the  
48 upper 400 km in the 3D structure to decrease the computational cost and memory usage. Using  
49 this minimum  $V_s$  gives  $h$  of 600 m and 300 m for 0.25 Hz and 0.50 Hz simulation, respectively.  
50 We use 'refinement' command in SW4 to increase the grid spacing with depth to reduce  
51 computational cost since the velocity increases with depth and the velocity model becomes  
52 more homogeneous with depth.

53 To maintain similar PPW for each block in the block boundary, we plot a profile of the  $V_s$  at  
54 different points in the 3D structure to determine optimal location of the block boundaries,  
55 usually where the  $\min V_s$  doubles (Fig. S5). The figure shows that the  $\min V_s$  increases to about  
56 2800 m/s below 25 km and stays constant with depth to 200 km depth. This is due to the lower  
57 velocity value of the subducting slab compares with the surrounding higher velocity rocks with  
58 depth. We setup refinement level at 75 depth. For the 0.50 Hz simulations, for example, we use

59 a curvilinear mesh of 300 m grid size in the upper 30 km depth, and Cartesian mesh below 30  
60 km with a grid spacing of 300 m in the upper 30 – 75 km depth and 600 m from 75-200 km  
61 depth.

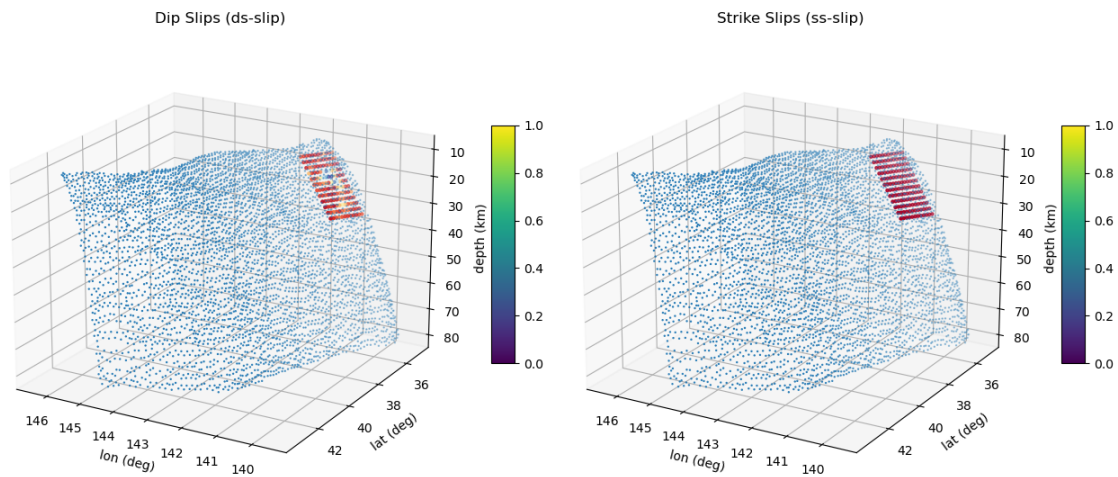
62 **Supplementary Figures**



63  
64 Fig. S1: Fault mesh of the Slab 2.0 model of Kuril region of the Japan Trench using GMSH. Each  
65 triangle shows the subfaults and the different colors show the partition of the Japan Trench for  
66 determining regular and undistorted mesh, but do not have any geological inference.

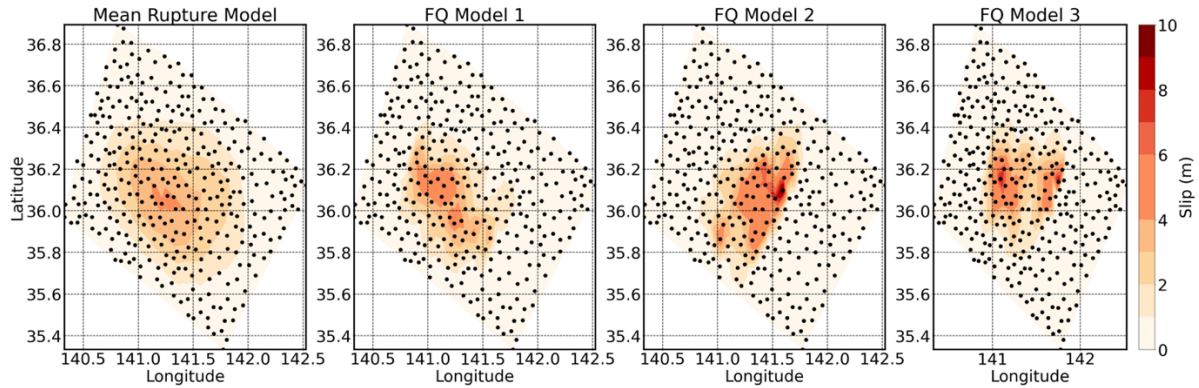
67

Ibaraki2011\_SRCMOD Finite Fault Model

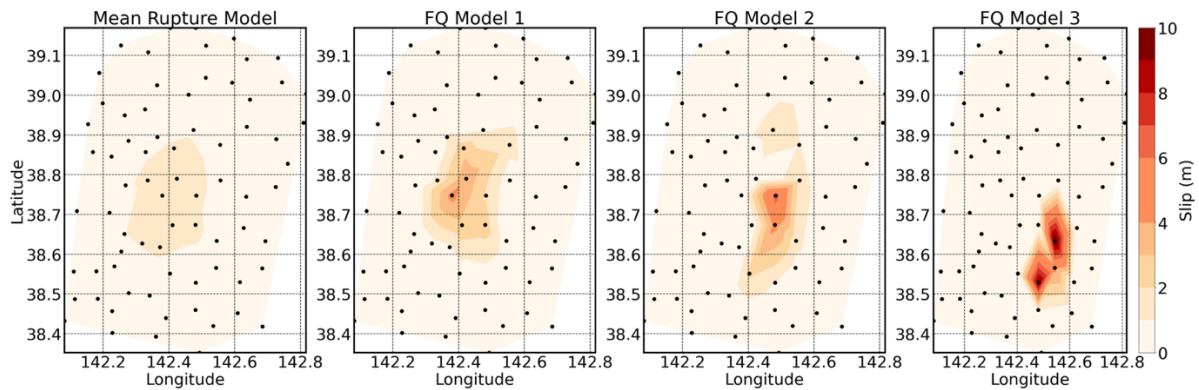


68  
69 Fig. S2: Mapping of the planar Ibaraki 2011 SRCMOD rupture (Kubo et al., 2013) on the non-  
70 planar Japan trench geometry from Slab 2.0 model. Blue dots represent the location of the  
71 center of each subfault outlining the Japan Trench while the square pattern regions in the two  
72 subplots show the dip and strike slips of the Ibaraki 2011 SRCMOD rupture model, respectively.

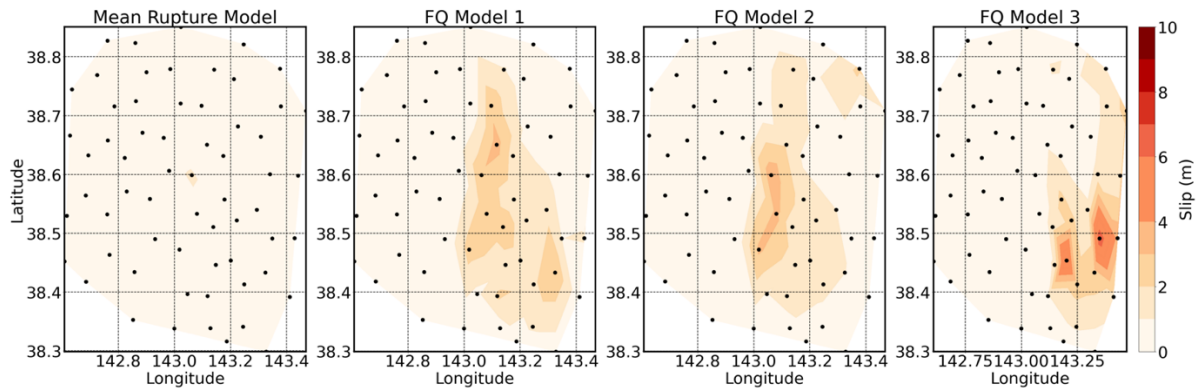
### Ibaraki 2011 (Zheng Rupture Model)



### Miyagi 2011 (Hayes Rupture Model)



### Miyagi 2011 (Zheng Rupture Model)



73

74

75

76

77

78

79

Fig. S3: Mean rupture model for Ibaraki 2011 (Zheng model), Miyagi 2011 (Hayes and Zheng

models), and three examples of the 100 FakeQuake random realization of the mean models.

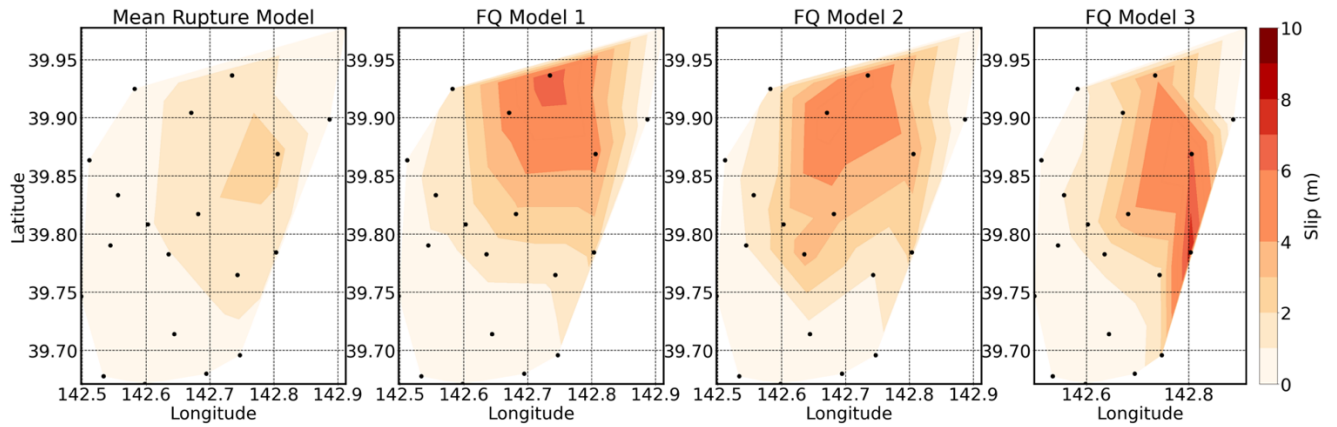
The color indicates the amount of slip per subfault, and the black dots signify the center of each

subfault. The slip is bigger overall in the FakeQuake models compared to the mean slip model in

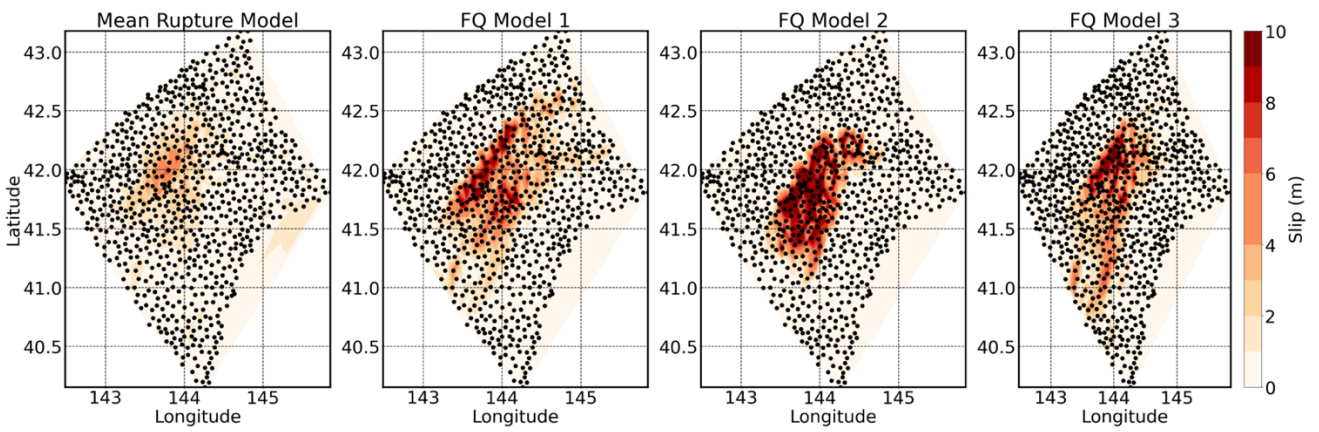
the top left to conserve the moment release in response to the change in rigidity at the subfault

locations compared to the one used to generate the mean slip model.

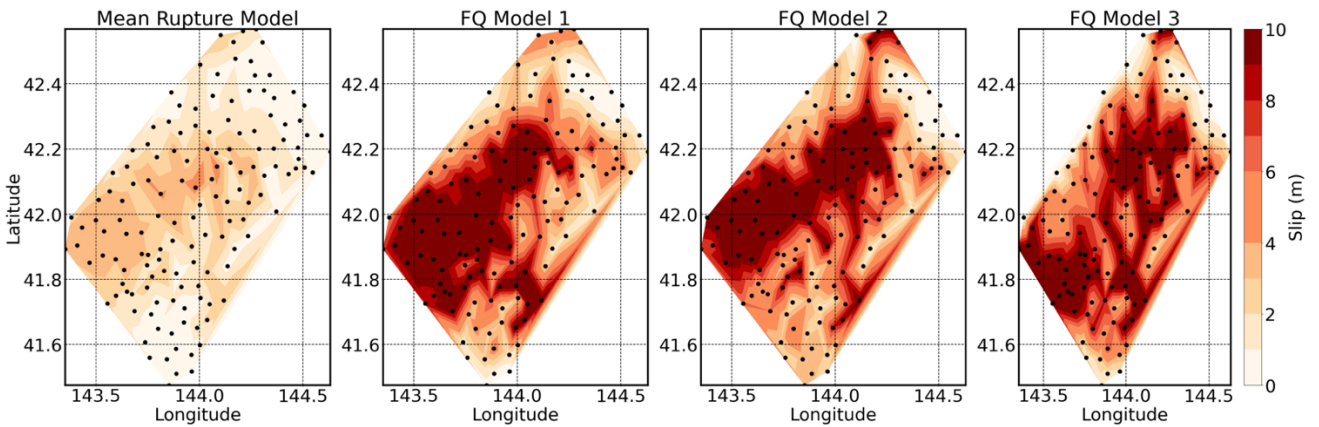
### Iwate 2011 (Zheng Rupture Model)



### Tokachi 203 (Hayes Rupture Model)



### Tokachi 2003 (SRCMOD3 Rupture Model)

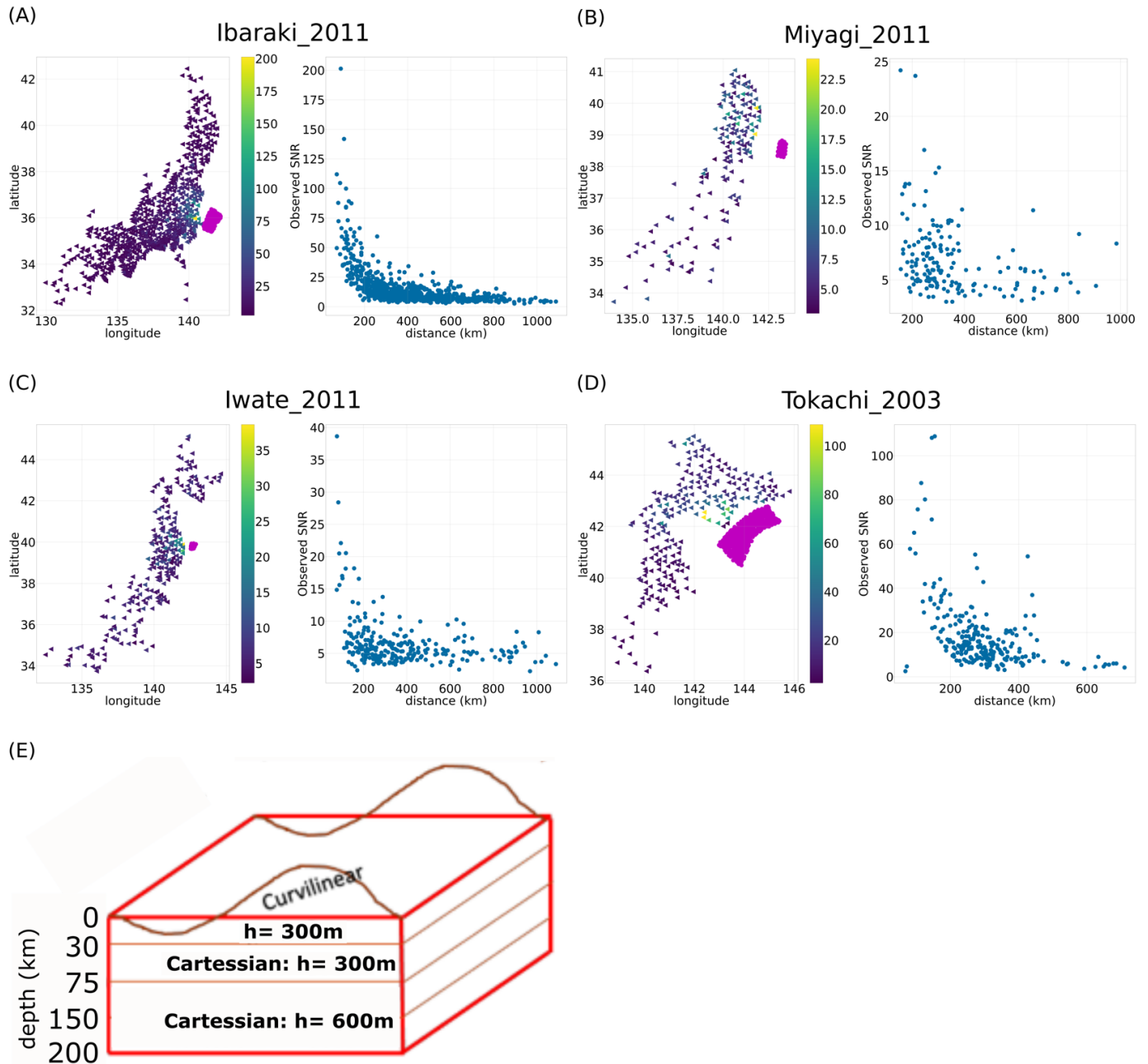


80

81 Fig. S4: Same as Figure S3, but for Iwate 2011 (Zheng model), Tokachi 2003 (Hayes and  
82 SRCMOD models).

83

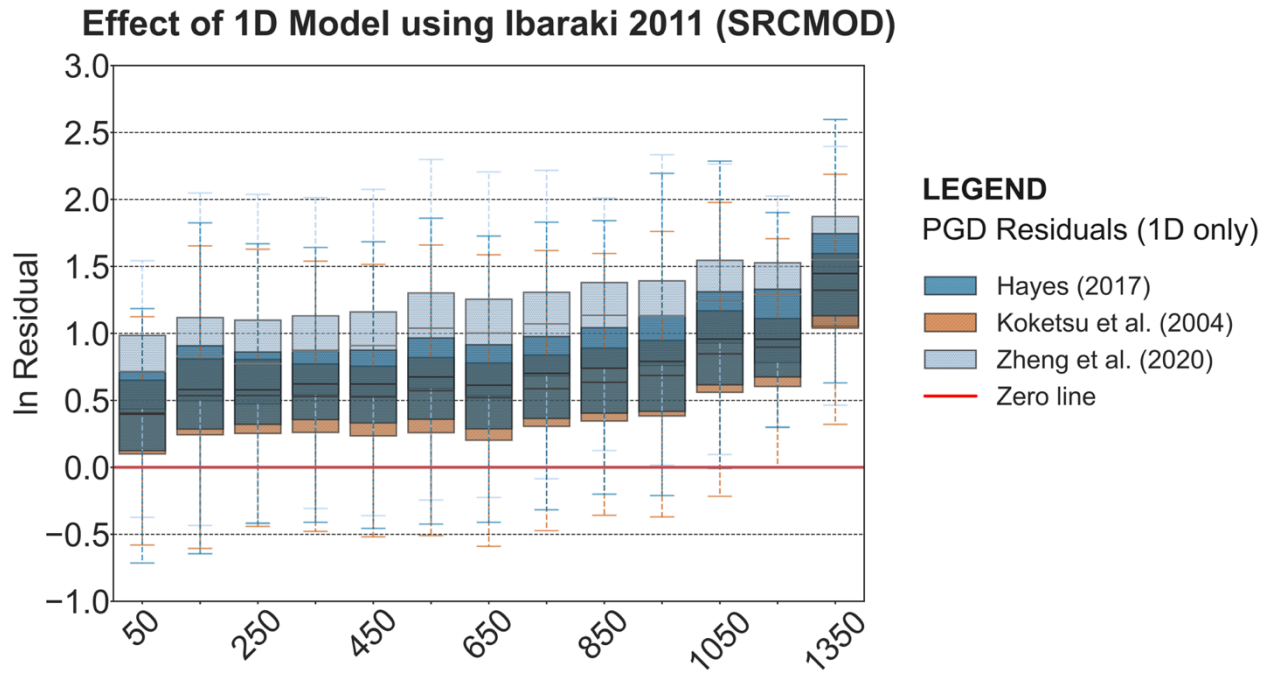




84

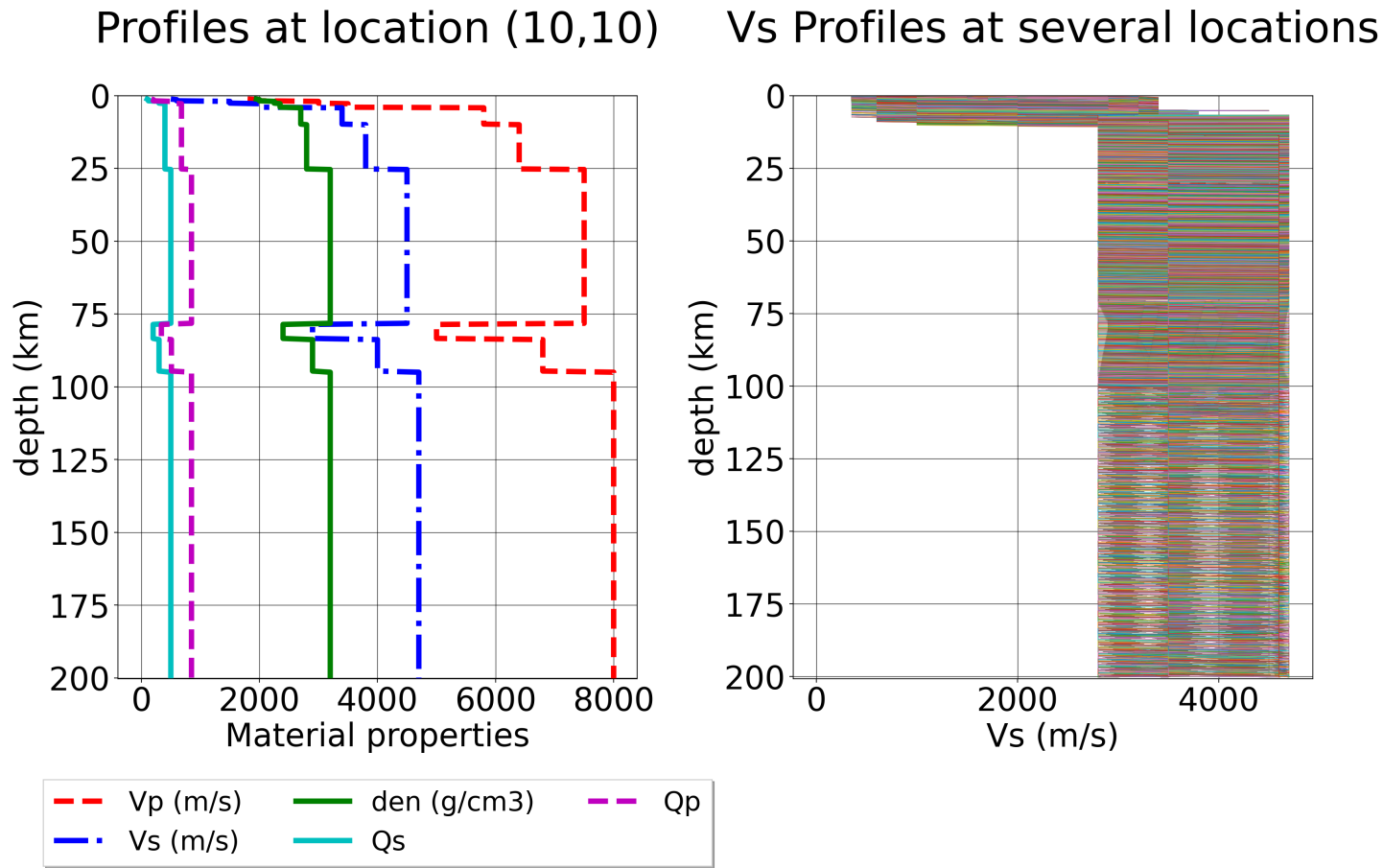
85 Fig. S5: SW4 domain for the 0.50 Hz simulations showing the (A-D) selected GNSS stations  
 86 (colored by the observed signal-to-noise ratio) and surface-projection of the FakeQuake  
 87 ruptures for each earthquake, and the observed Signal-to-Noise ratio (SNR) with distance.

88 Figure S5E shows the domain geometry showing the grid spacing, the refinement layer and  
 89 types of mesh used in the simulations. We used a curvilinear mesh for the topography/  
 90 bathymetry to a depth of 30 km, and cartesian mesh below 30 km with 300 m grid spacing from  
 91 30-75 km depth, and 600 m from 75 – 200 km depth.



93

94 Figure S6: Effect of the choice of 1D velocity model used for the 1D simulations on PGD  
 95 residuals using three 1D velocity models used by two other researchers: Zheng et al. (2020) and  
 96 Koketsu et al. (2004). On each boxplot, residuals for each model are shown as patterned box  
 97 and whisker plots. The blue, orange and light blue boxplots represent the PGD residuals for  
 98 Hayes (20017), Koketsu et al. (2014) and Zheng et al. (2020) studies, respectively. The red  
 99 horizontal line represents the zero residual line.



101

102

103

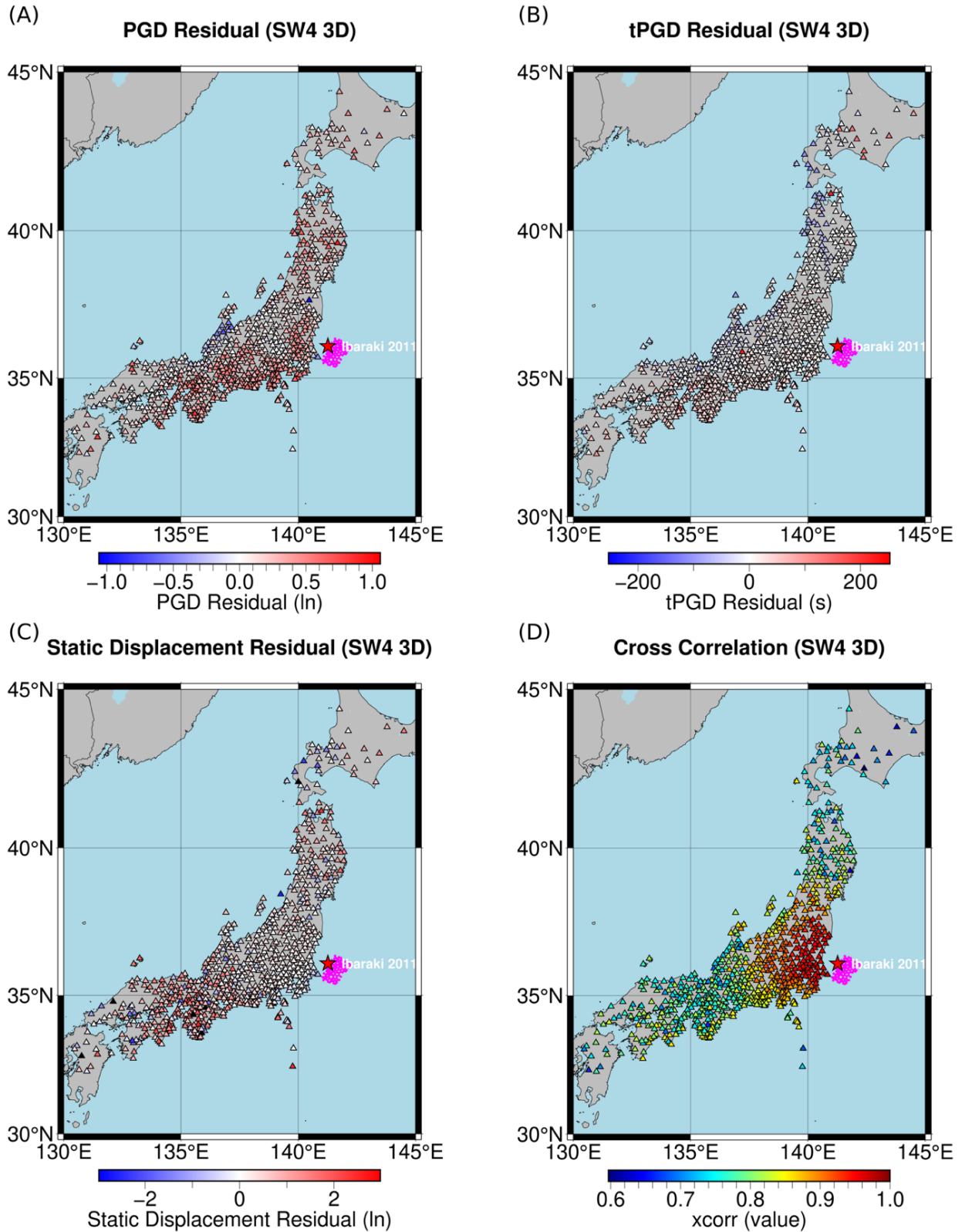
104

105

106

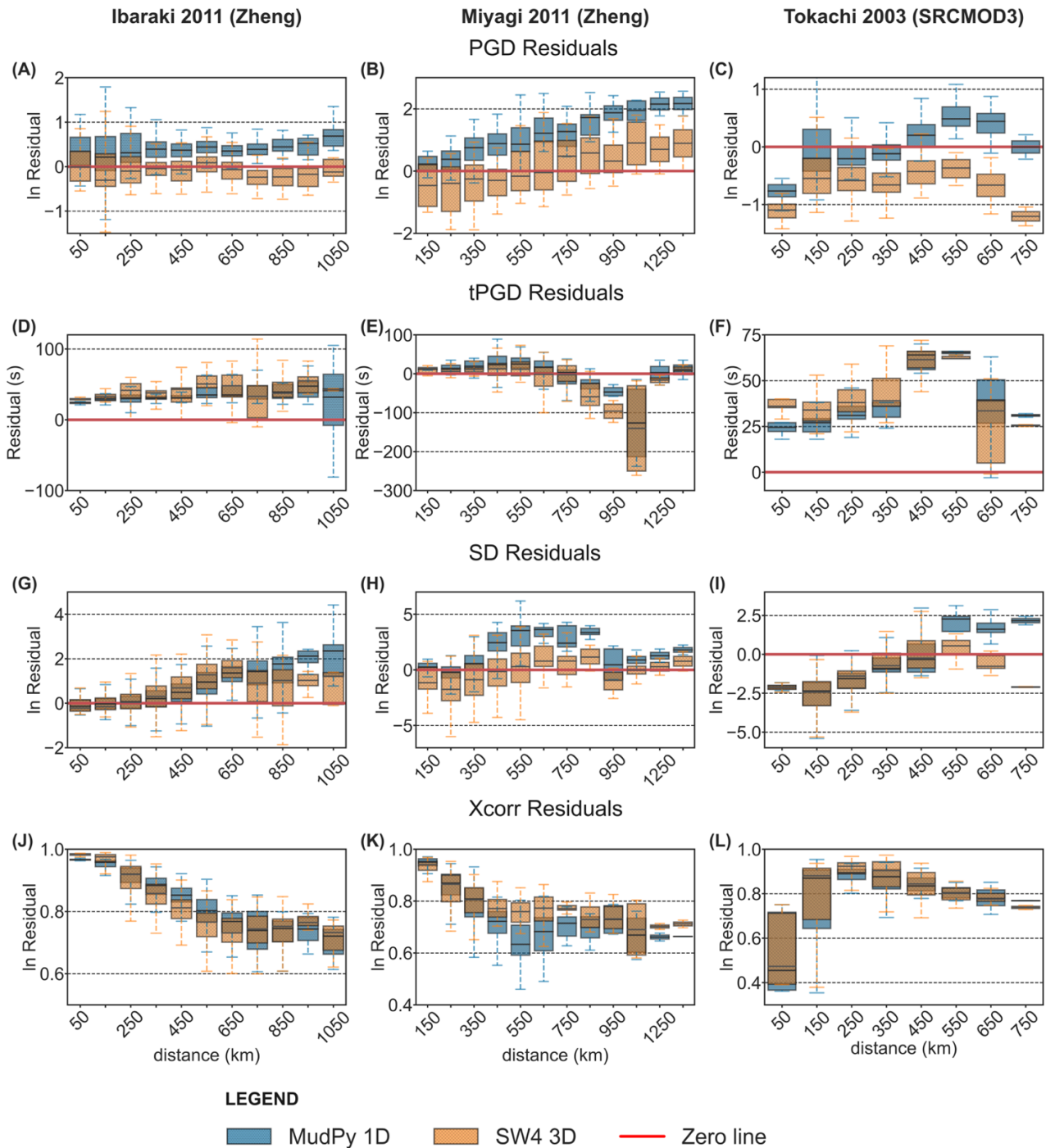
Fig. S7: (left) Profiles of the material properties at location  $x=10$  km and  $y= 10$  km in the 3D Japan Integrated Velocity Structure Model (Koketsu et al., 2008, 2009), while (right) shows all the Vs profiles at different locations within the 3D structure showing the variation of minimum shear wave velocity with depth.





107  
108  
109  
110

Fig. S8: The PGD,  $t_{PGD}$ , SD residuals and cross correlation map showing the spatial variation of the 3D residuals for the Ibaraki 2011 earthquake for Rupture 5 of the 100 FakeQuake ruptures using the SRCMOD mean rupture model (Kubo et al., 2013).



111

112 Fig. S9: Comparing MudPy 1D vs SW4 3D residuals between the synthetic to observed GNSS  
113 waveforms for Ibaraki 2011 (Zheng), Miyagi 2011 (Zheng) and Tokachi 2003 (SRCMOD3). Figure  
114 (A-C) PGD residuals, (D-F)  $t_{PGD}$  (s) residuals, (G-I) static displacement residuals and (J-L) cross  
115 correlation values. We compare only the residuals of two corresponding rupture models in the  
116 MudPy and SW4 synthetic simulations. The blue boxplots with circle hatched style represents  
117 the MudPy 1D residuals while the orange boxplot (diamond hatch style) represents the SW4 3D  
118 simulation. The red horizontal line represents the zero residual line.

119 Table S1: P- and S-wave velocities ( $V_p$  and  $V_s$ ), density ( $\rho$ ) and P- and S-wave quality factors ( $Q_p$   
 120 and  $Q_s$ ) for the 23 layers in the 3D Japan Integrated Velocity Structure Model (Koketsu et al.,  
 121 2008, 2009).

Layer number	P-wave velocity (m/s)	S-wave velocity (m/s)	Density ( $\text{kg/m}^3$ )	P-wave quality factor ( $Q_p$ )	P-wave quality factor ( $Q_s$ )
1	1700	350	1800	119	70
2	1800	500	1950	170	100
3	2000	600	2000	204	120
4	2100	700	2050	238	140
5	2200	800	2070	272	160
6	2300	900	2100	306	180
7	2400	1000	2150	340	200
8	2700	1300	2200	442	260
9	3000	1500	2250	510	300
10	3200	1700	2300	578	340
11	3500	2000	2350	680	400
12	4200	2400	2450	680	400
13	5000	2900	2600	680	400
14	5500	3200	2650	680	400
15	5800	3400	2700	680	400
16	6400	3800	2800	680	400
17	7500	4500	3200	850	500
18	5000	2900	2400	340	200
19	6800	4000	2900	510	300
20	8000	4700	3200	850	500
21	5400	2800	2600	340	200
22	6500	3500	2800	510	300
23	8100	4600	3400	850	500